Half-lives of cluster radioactivity with a generalized liquid-drop model

X J Bao, H F Zhang and B S Hu

School of Nuclear Science and Technology, Lanzhou University, Lanzhou 730000, People's Republic of China

G Royer

Laboratoire Subatech, UMR: IN2P3/CNRS-Université-Ecole des Mines, Nantes 44, France

J Q Li

Institute of Modern Physics, Chinese Academy of Sciences, Lanzhou 730000, People's Republic of China

Abstract. Half-lives of cluster radioactivity treated as very asymmetric spontaneous fission are investigated by the WKB barrier penetration probability. The potential barrier is constructed by a generalized liquid-drop model(GLDM), taking into account the nuclear proximity, the mass asymmetry, the accurate nuclear radius, the phenomenological pairing correction, and the microscopic shell correction. The calculated cluster emission half-lives reproduce accurately the experimental data. Predictions are provided for possible cluster radioactivity within the GLDM using the up-to-data atomic mass table AME2011, which may be used for the future experiments.

1. Introduction

Cluster radioactivity by heavy nuclei with an emitted cluster heavier than an α particle but lighter than fission fragments was first theoretically predicted in the beginning of the 1980s by Sandulescu, Poenaru and Greiner[1]. In 1984, the emission of ^{14}C nucleus by ^{223}Ra was observed[2, 3]. Sine then, other cluster radioactivities have been observed leading to ^{14}C ,^{20}O, ^{23}F, $^{22,24-46}Ne$, $^{28,30}Mg$, and $^{32,34}Si$ emission, and their partial half-lives have been measured. The probability of cluster radioactivity is strongly related to the shell effects. Indeed, the Q value plays an important role in cold nuclear decay with the emission of charged particles. The shortest value of half-life for cluster radioactivity is obtained when the heavy daughter nucleus is a double-magic nucleus. Several theoretical approaches can be employed to investigate cluster emission: the superasymmetric fission model[4, 5, 6, 7], which is based on *Gamow's* idea of barrier penetration; among them the preformed cluster model(PCM)[8, 9, 10], in which the cluster is assumed to be preformed in the parent nucleus and the preformation factor for all possible clusters is calculated by solving the Schrödinger equation for the dynamical flow of mass and charge; and a cluster model with a mean-field cluster potential can also provide a good description of cluster emission[11]. The conventional liquid-drop model was developed to include the nuclear proximity energy and a quasi-molecular shapes by G.Royer in 1984, which allows us to describe the fusion, the fission, cluster radioactivity, α-decay and proton emission processes[12, 13, 14, 15, 16, 17, 18, 19]. The cluster radioactivity was firstly calculated by the GLDM in 1998 years[23]. The experimental data was reproduced reasonably and the largest deviation between the calculated half-lives and experimental data is about 3 orders of magnitude. Recently, this calculation was improved by introducing the preformation factors of cluster in the mother nucleus[24], $P_0^C = (P_0^\alpha)^{(A_2-1)/3}$, where A_2 is the mass number of the cluster and P_0^α is the preformation factor for α-decay. The calculated results coincide with experimental data within 2 orders of magnitude[20]. In these previous calculations, the shell correction and pairing correction are not considered. It is well know that the shell effects play a key role for cluster radioactivity. So it is very interesting to check how much the shell effects and pairing correction contribute to the potential barrier as well as the half-life for cluster radioactivity, which is our major motivation of this work.

The paper is organized as follows. The features of quasi-molecular shapes are given in section 2, the details of the GLDM taking into account the pairing and shell corrections are described in section 3. In section.4, the cluster radioactivity half-lives have been computed by using the WKB. In section.5, the results and discussions are presented. A summary is given in section.6.

2. Quasi-molecular shapes

The shape is given simply in polar coordinates (in the plane $\phi = 0$) by[21]

$$R(\theta)^2 = \begin{cases} a^2 \sin^2\theta + c_1 \cos^2\theta & 0 \le \theta \le \pi/2 \\ a^2 \sin^2\theta + c_2 \cos^2\theta & \pi/2 \le \theta \le \pi \end{cases}$$

where c_1 and c_2 are the two radial elongations and a the neck radius. Assuming volume conservation, the two parameters $s_1 = a/c_1$ and $s_2 = a/c_2$ completely define the shape. The radii of the future fragments allows to connect s_1 and s_2:

$$s_2^2 = \frac{s_1^2}{s_1^2 + (1 - s_1^2)(R_2/R_1)^2}, \tag{1}$$

when s_1 decreases from 1 to 0 the shape evolves continously from one sphere to two touching spheres with the natural formation of a deep neck while keeping almost spherical ends. So, we would like to point out that the most attractive feature of the quasi-molecular shapes is that it can describe the process of the shape evolution from one body to two separated fragments in a unified way.

3. Potential energy

The total energy of a deformed nucleus is the sum of the GLDM energy and the shell and pairing energies.

3.1. GLDM energy

Within this GLDM the macroscopic energy of a deformed nucleus is defined as[25]

$$E = E_V + E_S + E_C + E_{prox} + E_{rot}, \tag{2}$$

where the different terms are respectively the volume, surface, Coulomb, nuclear proximity and rotational energies.
For one-body shapes, the volume E_V, surface E_S and Coulomb E_C energies are given by

$$E_V = -15.494(1 - 1.8I^2)A \ MeV, \tag{3}$$

$$E_S = 17.9439(1 - 2.6I^2)A^{2/3}(S/4\pi R_0^2) \ MeV, \tag{4}$$

$$E_C = 0.6e^2(Z^2/R_0)B_C \ MeV. \tag{5}$$

B_C is the Coulomb shape dependent function, S is the surface and I is the relative neutron excess.

$$B_C = 0.5 \int (V(\theta)/V_0)(R(\theta)/R_0)^3 \sin\theta d\theta, \tag{6}$$

where $V(\theta)$ is the electrostatic potential at the surface and V_0 the surface potential of the sphere. The effective sharp radius R_0 has been chosen as

$$R_0 = 1.28A^{1/3} - 0.76 + 0.8A^{-1/3} \ fm. \tag{7}$$

this formula proposed in Ref.[22] is derived from the droplet model and the proximity energy and simulates rather a central radius for which $R_0/A^{1/3}$ increases slightly with the mass. It has been shown[13, 14] that this selected more elaborated expression can also be used to reproduce accurately the fusion, fission and cluster and alpha decay data.
when the fragment are separated[23],

$$E_V = -15.494[(1 - 1.8I_1^2)A_1 + (1 - 1.8I_2^2)A_2]\ MeV, \tag{8}$$

$$E_S = 17.9439[(1 - 2.6I_1^2)A_1^{2/3} + (1 - 2.6I_2^2)A_2^{2/3}]\ MeV, \tag{9}$$

$$E_C = 0.6e^2Z_1^2/R_1 + 0.6e^2(Z_2^2/R_2) + e^2Z_1Z_2/r\ MeV. \tag{10}$$

To ensure volume conservation, R_1 and R_2 read

$$R_1 = R_0(1 + \beta^3)^{-1/3}, \tag{11}$$

$$R_2 = R_0\beta(1 + \beta^3)^{-1/3}, \tag{12}$$

where,

$$\beta = \frac{1.28A_1^{1/3} - 0.76 + 0.8A_1^{-1/3}}{1.28A_2^{1/3} - 0.76 + 0.8A_2^{-1/3}}. \tag{13}$$

The discontinuity of a few MeV appearing at the contact point due to the difference between A_1/Z_1 and A_2/Z_2 has been linearized from the contact point to the sphere since it originates form discarding the charge rearrangement in the nuclear matter which occurs progressively. The surface energy comes from the effects of the surface tension forces in a half space. When a neck or a gap appears between separated fragments an additional term called proximity energy must be added to take into account the effects of the nuclear forces between the close surface. It moves the barrier top to an external position and strongly decreases the pure Coulomb barrier:

$$E_{prox}(r) = 2\gamma \int_{h_{min}}^{h_{max}} \Phi[D(r,h)/b]2\pi h dh \tag{14}$$

where

$$\gamma = 0.9517\sqrt{(1 - 2.6I_1^2)(1 - 2.6I_2^2)}\ \ MeVfm^{-2} \tag{15}$$

r is the distance between the mass centres, h is the transverse distance varying from the neck radius or zero to the height of the neck border, D is the distance between the opposite surfaces in consideration and b is the surface width fixed at 0.99 fm. Φ is the proximity function. The surface parameter γ is the geometric mean between the surface parameters of the two fragments.

3.2. Shell energy

The shape-dependent shell corrections have been determined within the Droplet Model expressions[25]:

$$E_{shell} = E_{shell}^{sphere}(1 - 2.6\alpha^2)e^{-\alpha^2} \tag{16}$$

where, the range a has been chosen to be $0.32r_0$. $\alpha^2 = (\delta R)^2/a^2$, the factor α^2 is the Myers-Swiatecki measure for the deformation of the nucleus. The attenuating factor $(e^{-\alpha^2})$makes the whole shell correction energy decrease from maximum to zero with increasing distortion of the nucleus. The distortion is the root-mean-square value of the deviation of the radius vector $R(\theta.\phi)$, specifying the nuclear surface,

$$(\delta R)^2 = \frac{\int\int (R - R_0)^2 d\Omega}{\int\int d\Omega} \tag{17}$$

The E_{shell}^{sphere} is shell corrections for a spherical nucleus,

$$E_{shell}^{sphere} = cE_{sh} \tag{18}$$

is obtained by the traditional Strutinsky procedure by setting the smoothing parameter $\gamma = 1.15\hbar\omega_0$ and the order $p = 6$ of the Gauss-Hermite polynomials, where $\hbar\omega_0 = 41A^{-1/3}$ MeV is the mean distance between the gross shells.[26] the sum of the shell energies of protons and neutrons. Meanwhile, we introduce a scale factor c to the shell correction. In this work, we choose c value of 0.62. To obtain the shell correction E_{shell}^{sphere}, we calculate the single-particle levels with an axially deformed Woods-Saxon potential and then execute the Strutinsky procedure. The single-particle Hamiltonian is written as,

$$H = T + V + V_{S.O}, \tag{19}$$

with the spin-orbit potential

$$V_{S.O} = -\lambda(\frac{\hbar}{2Mc})^2 \nabla V \cdot (\vec{\sigma} \times \vec{p}), \tag{20}$$

where M is the free nucleonic mass, $\vec{\sigma}$ is the Pauli spin matrix and $\vec{p}$ is the nucleon momentum. λ means the strength of the spin-orbit potential. In this work, we set $\lambda = \lambda_0(1 + N_i/A)$ with $N_i = Z$ for protons and $N_i = N$ for neutrons and λ_0 value of 26.3163. The central potential V is descried by an axially deformed Woods-Saxon form

$$V(\vec{r}) = \frac{V_q}{1 + \exp[\frac{r - R(\theta)}{a}]}, \tag{21}$$

where the depth V_q of the central potential(q=p for protons and q=n for neutrons)is written as

$$V_q = V_0 \pm V_S I, \tag{22}$$

with the plus sign for neutrons and the minus sign for protons. V_0 and a are value of -47.4784 and 0.7842, respectively. V_S and I are the isospin-asymmetric part of the potential depth and the relative neutron excess.
where

$$V_S = c_{sym}[1 - \frac{\kappa}{A^{1/3}} + \frac{2 - |I|}{2 + |I|A}] \tag{23}$$

The values of c_{sym} and κ are 29.2876 and 1.4492, respectively[27].

3.3. Pairing energy

The shape-dependent pairing energy has been calculated with the following expressions of the finite-range droplet model.[28]
For odd Z, odd N nuclear:

$$E_{Pairing} = \frac{4.8B_S}{N^{1/3}} + \frac{4.8B_S}{Z^{1/3}} - \frac{6.6}{B_S A^{2/3}} \tag{24}$$

For odd Z, even N nuclear:

$$E_{Pairing} = \frac{4.8B_S}{Z^{1/3}} \tag{25}$$

For even Z, odd N nuclear:

$$E_{Pairing} = \frac{4.8B_S}{N^{1/3}} \tag{26}$$

For even Z, even N nuclear:

$$E_{Pairing} = 0 \tag{27}$$

The relative surface energy B_s, which is the ratio of the surface area of the nucleus at the actual shape to the surface area of the nucleus at the spherical shape, is give by

$$B_s = \frac{\int_S dS}{S_{sphere}} \tag{28}$$

The pairing energies vary with B_s.

4. Experimental and theoretical half-lives

In the unified fission model, the decay constant of the parent nucleus is simply defined as[23],

$$\lambda = \upsilon_0 P \tag{29}$$

The assault frequency υ_0 has been taken as,

$$\upsilon_0 = 2.5 \times 10^{20} s^{-1} \tag{30}$$

The barrier penetrability P is calculated within the action integral

$$P = \exp[-\frac{2}{\hbar}\int_{R_{in}}^{R_{out}} \sqrt{2B(r)(E(r) - E(sphere))}dr], \tag{31}$$

with $E(R_{in}) = E(R_{out}) = Q_{exp}$. The inertia $B(r)$ has been chosen as,

$$B(r) = \mu\{1 + f(r)\frac{272}{15}\exp[-\frac{128}{51}((r - R_{in})/R_0)]\}. \tag{32}$$

where

$$f(r) = \begin{cases} (\frac{R_{cont}-r}{R_{cont}-R_{in}})^2 & r \le R_{cont} \\ 0 & r \ge R_{cont} \end{cases}$$

Where R_{cont} is the sum of R_1 and R_2. The partial half-life is related to the decay constant λ by

$$T_{1/2} = \frac{\ln 2}{\lambda}. \tag{33}$$

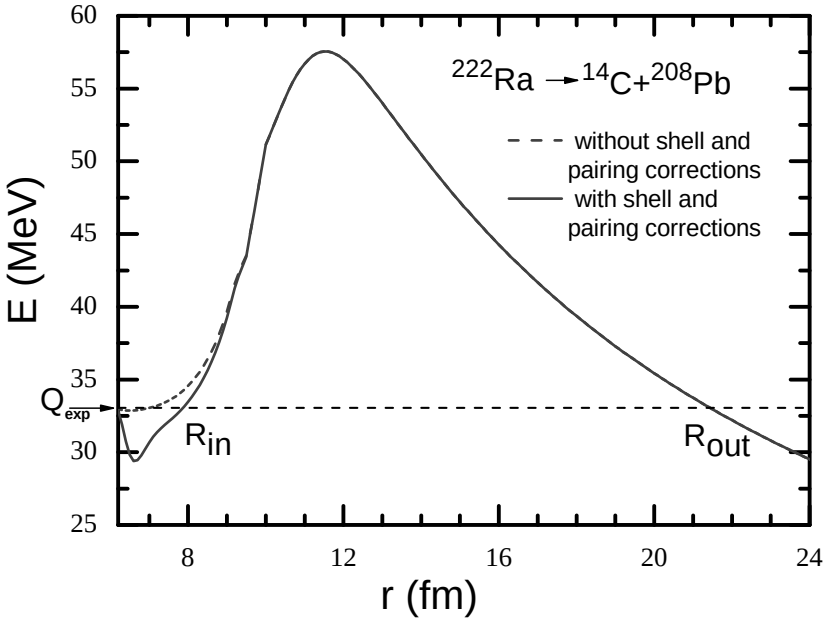

Figure 1. Potential barrier including a nuclear proximity energy term corrections versus emission of ^{14}C from the ^{222}Ra mother nucleus. The dashed and solid lines correspond to the results without and with the shell corrections and the pairing effects energy term, respectively. $R_{\rm in}$ and $R_{\rm out}$ are the inner and outer turning points and r is the distances between the mass centers .

5. Results and discussions

The numerical results are given in table 1, in which the second column denotes Q values. The results calculated by the GLDM without and with taking into account the microscopic shell corrections and the pairing effects are listed in the third and fourth columns. The experimental cluster emission half-lives [30, 31] are given in the fifth column. It can be found from the fourth and fifth columns in table 1 that the deviations between the experimental data and the calculated values are less than 10^2 for the most nuclei. As can be seen from the table 1, although the cluster radioactivity half-lives span many orders of magnitude from 10^{11} to 10^{29} s, the calculated half-lives agree precisely with the experimental ones and the ratio between them is approximately within a factor of 10. For the total 33 clusters emission considered in this work, we reproduce the experimental half-lives of 28 clusters emission within a factor 10^1, and 5 clusters emission within a factor 10^2.

For comparison, in the last column of table 1 are shown the corresponding results of S.N.Kuklin work [33] in which the cluster spectroscopic factors were calculated by solving the Schrödinger equation in charge asymmetry coordinates, and the decay of the cluster configuration was treated by tunneling through the barrier in the nucleus-nucleus potential within the WKB method [33]. It is found that the results of S.N.Kuklin et al [33], except for the case of ^{14}C from ^{224,226}Ra, agree well with the experimental ones. So except for the case of ^{14}C from ^{224,226}Ra, the results from GLDM and S.N.Kuklin

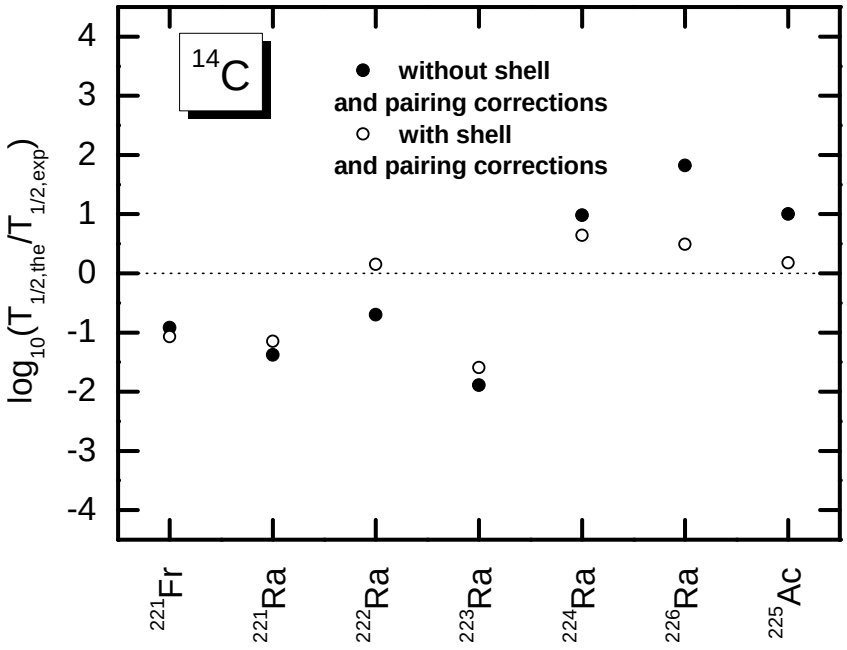

Figure 2. Deviations between the logarithms of the calculated half-lives and the experimental values for ^{14}C cluster radioactivity from different parent nuclei.

et al [33] are all consistent with the experimental observations. In addition, we have previously [23] calculated cluster emission half-lives within a generalized liquid drop model taking into account the nuclear proximity, the mass asymmetry and the accurate nuclear radius in adding the shell and pairing effects empirically. The theoretical cluster emission half-lives generally agree well with the experimental results. For many nuclei, the experimental half-lives are reproduced within a factor of 10. However, the empirically shell corrections relate to the magic numbers. So in our calculations here, the potential barriers have been constructed by using GLDM where the proximity effects, the pairing effects and the microscopic shell corrections are included. To obtain the microscopic shell correction, we calculate the single-particle levels based on an axially deformed Woods-Saxon potential and then apply strutinsky method. By comparing the present results of cluster emission half-lives with the results from the previously work [23], we would like to point out that the present calculation gives better agreement with experimental data.

From table 1, one of the interesting facts is that the half-life ^{14}C cluster emission from different parent nuclei decreases while the Q value increasing. More generally, one can observe that the half-life of the same cluster emission from different parent nuclei half-life decreases when the Q value increasing. The sensitivity of half-life with the Q value has already been pointed out by Poenaru et al [34] in the case of ^{12}C emission from ^{114}Ba. Therefore, the Q value is a key factor for the cluster radioactivity half-life

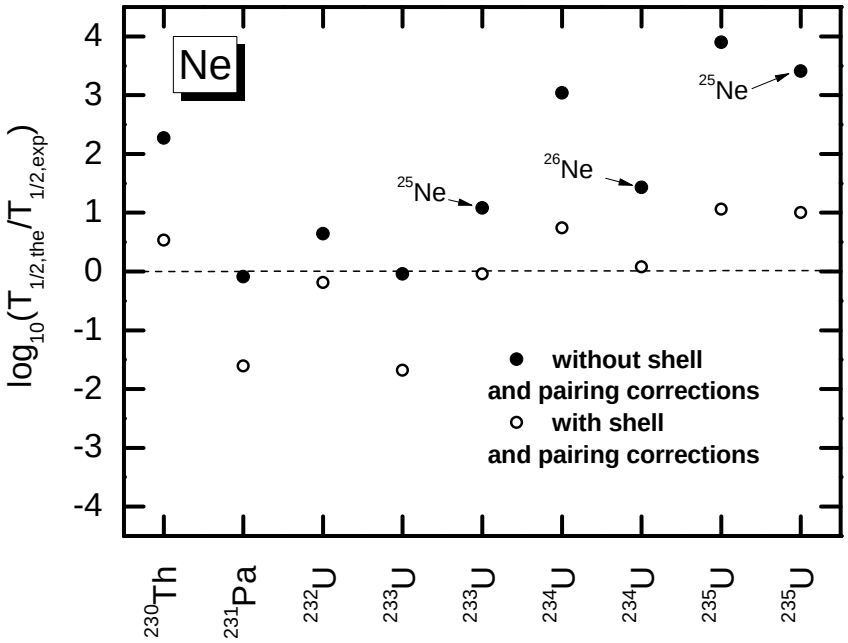

Figure 3. The same as Fig. 2, but for Ne cluster radioactivity.

calculation. From calculations, it is found that the half-life is extremely sensitive to the Q value. Even an uncertainty of 1 MeV in Q can leads to an uncertainty of cluster emission half-life ranging from 10^2 to 10^3 times.

The potential barrier governing the ^{14}C emission from ^{222}Ra is displayed in Fig. 1. The dashed and solid curve show the potential barrier relatively to the sphere without and with the microscopic shell corrections and the pairing effects, respectively. One can see clearly from Fig. 1 that R_{in} changes owing to taking into account the shell correction and pairing effect. This will directly affect the half-lives of cluster emission. To illustrate the agreement for ^{14}C cluster emission between our calculations and the experimental data clearly, the comparison of the calculated cluster emission half-lives with the experimental data is shown in Fig. 2, in which the open and solid circles indicate the results of GLDM with and without the microscopic shell corrections and the pairing effects, respectively. It can be seen that the values of $\log_{10}(T^b_{1/2}(\text{cal.})/T_{1/2}(\text{exp.}))$ are generally within the range of about -1.5-0.6, which corresponds to the values of the ratio $T^b_{1/2}(\text{cal.})/T_{1/2}(\text{exp.})$ within the range of about 0.03-0.45. This means that the calculated cluster emission half-lives are in good agreement with the experimental data for ^{14}C cluster emission from different parent nuclei. However, when the microscopic shell correction and the pairing effect contributions are not considered, the values of $\log_{10}(T^a_{1/2}(\text{cal.})/T_{1/2}(\text{exp.}))$ are within the range of about -1.9-1.8, which corresponds to the values of the ratio $T^a_{1/2}(\text{cal.})/T_{1/2}(\text{exp.})$ within the range of about 0.01-66.7. Therefore we would like to point out that the shell effect and pairing correction play a

important role for the half-life of cluster radioactivity.

In order to illustrate the half-lives of cluster radioactivity influenced by the shell and pairing effects, we shown in Fig.3 the variation of the deviations between experimental half-lives and theoretical ones ($\log_{10}(T^b_{1/2}(\text{cal.})/T_{1/2}(\text{exp.}))$) with various Ne cluster radioactivity from different parent nuclei. The open and solid circles indicate the results of GLDM with and without the microscopic shell corrections and the pairing effects, respectively. One can see that the absolute values of $\log_{10}(T^b_{1/2}(\text{cal.})/T_{1/2}(\text{exp.}))$ are generally less than 1.00. Which means that the experimental Ne cluster radioactivity half-lives are well reproduced. Whereas in the case where the shell and pairing energies are not included, the maximum deviation in the present cluster radioactivity half-life with experimental value is found for ^{24}Ne emission from the ^{235}U up to 4 orders of magnitude. Based on above precisely agreement between the results of GLDM taking into account the microscopic shell effect and the shape-dependent pairing energy and the experimental data, we would like to point out that the role of the microscopic corrections and the pairing energy are emphasized since their introduction allows us to reproduce the potential barrier characteristics which govern the half-lives.

The calculated values of half-lives for the emission of various clusters from the actinide parent nuclei are shown in Table 2. Possible candidates for future experiments, which have half-lives to be measurable with present experimental setups. Because the calculated half-lives are agree precisely with the experimental ones, if they exist, one can extend our calculations to provide reasonable estimates of the half-lives of parent nuclei with respect to the decays by cluster emission.

6. Summary and conclusion

In our approach the cluster radioactivity can be described in as a spontaneous tunneling process via quasi-molecular shapes like the asymmetric fission. The decay of radioactive nuclei which emit heavy clusters such as C, O, Ne, Mg and Si has been studied within a generalized liquid-drop model, in which the potential barrier have been determined within a generalized liquid drop model taking into account the microscopic shell corrections and the shape-dependent pairing energy. The cluster emission half-lives have been calculated within the WKB barrier penetration probability without introducing preformation factor. The calculated results reproduce accurately the experimental data. From calculations, it is found that the roles of the microscopic shell correction and pairing effect are emphasized since their introduction allows us to reproduce the potential barrier characteristics which govern the half-lives. The half-life is extremely sensitive to the Q value and an uncertainty of 1 MeV in Q corresponds to an uncertainty of cluster emission half-life ranging from 10^2 to 10^3 times. Predictions have been made for some possible cluster decay of actinide parent nuclei of half-lives, we presume that the present work will be a guide to future experiments.

Table 1. The Q values and the half-lives of cluster radioactivity. The second column denotes Q values extracted from [32]. The third and fourth columns indicate, respectively, the theoretical half-lives without and with taking into account the pairing effects and the microscopic shell corrections. The experimental data [31, 33] are shown in the fifth column and the results of Kuklin [34] are shown in the last column for comparison.

Emitter and cluster	Q_{exp} (MeV)	Theoretical $T^a_{1/2}$(cal.)(s)	Theoretical $T^b_{1/2}$(cal.)(s)	Experimental $T_{1/2}$(exp.)(s)	Ref[33]
^{221}Fr$\rightarrow^{14}$C+^{207}Tl	31.401	4.1×10^{13}	2.8×10^{13}	3.3×10^{14}	2.0×10^{15}
^{221}Ra$\rightarrow^{14}$C+^{207}Pb	32.507	1.0×10^{12}	1.7×10^{12}	2.4×10^{13}	2.6×10^{12}
^{222}Ra$\rightarrow^{14}$C+^{208}Pb	33.161	2.4×10^{10}	1.7×10^{11}	1.2×10^{11}	1.0×10^{11}
^{223}Ra$\rightarrow^{14}$C+^{209}Pb	31.941	2.5×10^{13}	5.1×10^{13}	2.0×10^{15}	7.2×10^{15}
^{224}Ra$\rightarrow^{14}$C+^{210}Pb	30.641	7.1×10^{16}	3.3×10^{16}	7.4×10^{15}	1.9×10^{18}
^{226}Ra$\rightarrow^{14}$C+^{212}Pb	28.313	1.2×10^{23}	5.6×10^{21}	1.8×10^{21}	4.3×10^{24}
^{225}Ac$\rightarrow^{14}$C+^{211}Bi	30.590	1.4×10^{18}	2.1×10^{17}	1.4×10^{17}	2.8×10^{18}
^{226}Th$\rightarrow^{14}$C+^{212}Po	30.662	1.4×10^{19}	2.0×10^{18}	$>2.0\times10^{15}$	
^{226}Th$\rightarrow^{18}$O+^{208}Pb	45.879	5.7×10^{19}	1.5×10^{18}	$>2.0\times10^{15}$	
^{228}Th$\rightarrow^{20}$O+^{208}Pb	44.870	2.3×10^{22}	4.4×10^{21}	7.5×10^{20}	2.5×10^{22}
^{230}Th$\rightarrow^{24}$Ne+^{206}Hg	57.944	8.3×10^{26}	1.5×10^{25}	4.4×10^{24}	5.2×10^{25}
^{232}Th$\rightarrow^{26}$Ne+^{206}Hg	56.103	2.4×10^{31}	5.6×10^{29}	$>1.6\times10^{29}$	
^{231}Pa$\rightarrow^{23}$F+^{208}Pb	52.036	1.9×10^{25}	1.8×10^{24}	1.0×10^{26}	7.6×10^{23}
^{231}Pa$\rightarrow^{24}$Ne+^{207}Tl	60.599	1.4×10^{23}	4.2×10^{21}	1.7×10^{23}	1.4×10^{20}
^{230}U$\rightarrow^{22}$Ne+^{208}Pb	61.579	8.0×10^{22}	2.3×10^{20}	$>1.6\times10^{18}$	
^{230}U$\rightarrow^{24}$Ne+^{206}Pb	61.543	1.5×10^{23}	9.3×10^{21}	$>1.6\times10^{18}$	
^{232}U$\rightarrow^{28}$Mg+^{204}Hg	74.537	6.8×10^{27}	7.9×10^{24}	$>4.5\times10^{22}$	
^{232}U$\rightarrow^{24}$Ne+^{208}Pb	62.497	1.1×10^{21}	1.6×10^{20}	2.5×10^{20}	5.9×10^{20}
^{233}U$\rightarrow^{24}$Ne+^{209}Pb	60.679	6.3×10^{24}	1.4×10^{23}	6.8×10^{24}	
^{233}U$\rightarrow^{25}$Ne+^{208}Pb	60.921	2.4×10^{24}	1.8×10^{23}	2.0×10^{23}	1.1×10^{24}
^{233}U$\rightarrow^{28}$Mg+^{205}Hg	74.451	8.0×10^{27}	1.5×10^{25}	$>3.9\times10^{27}$	
^{234}U$\rightarrow^{24}$Ne+^{210}Pb	59.020	1.8×10^{28}	8.8×10^{25}	1.6×10^{25}	
^{234}U$\rightarrow^{26}$Ne+^{208}Pb	59.609	2.1×10^{27}	9.3×10^{25}	7.9×10^{25}	4.8×10^{26}
^{234}U$\rightarrow^{28}$Mg+^{206}Hg	74.336	6.6×10^{27}	2.9×10^{25}	3.5×10^{25}	1.4×10^{24}
^{235}U$\rightarrow^{24}$Ne+^{211}Pb	57.555	2.2×10^{31}	3.2×10^{28}	2.8×10^{27}	
^{235}U$\rightarrow^{25}$Ne+^{210}Pb	57.902	7.3×10^{30}	2.8×10^{28}	2.8×10^{27}	
^{235}U$\rightarrow^{28}$Mg+^{207}Hg	72.382	3.1×10^{31}	3.3×10^{28}	$>2.8\times10^{28}$	
^{236}U$\rightarrow^{30}$Mg+^{206}Hg	72.509	8.1×10^{31}	1.5×10^{29}	3.8×10^{27}	2.0×10^{28}
^{237}Np$\rightarrow^{30}$Mg+^{207}Tl	75.029	5.5×10^{28}	1.6×10^{27}	$>3.7\times10^{27}$	
^{236}Pu$\rightarrow^{28}$Mg+^{208}Pb	79.897	2.6×10^{21}	2.9×10^{20}	4.7×10^{21}	5.5×10^{20}
^{238}Pu$\rightarrow^{28}$Mg+^{210}Pb	76.147	2.9×10^{28}	5.4×10^{25}	5.0×10^{25}	
^{238}Pu$\rightarrow^{30}$Mg+^{208}Pb	77.039	7.9×10^{26}	1.4×10^{25}	4.7×10^{25}	6.7×10^{25}
^{238}Pu$\rightarrow^{32}$Si+^{206}Hg	91.455	1.9×10^{28}	3.0×10^{25}	1.9×10^{24}	5.6×10^{27}

Table 2. Predicted values of half-lives the possible cluster decay of actinide parent nuclei.

Emitter and cluster	Q(MeV)	$T_{1/2}$(s)	Emitter and cluster	Q(MeV)	$T_{1/2}$(s)
^{220}Ra$\rightarrow^{12}$C+^{208}Pb	32.132	5.6×10^{11}	^{220}Ra$\rightarrow^{16}$O+^{204}Hg	39.843	3.8×10^{27}
^{221}Ra$\rightarrow^{15}$N+^{206}Tl	35.243	7.2×10^{21}	^{221}Ra$\rightarrow^{18}$O+^{203}Hg	39.160	3.3×10^{31}
^{222}Ra$\rightarrow^{15}$N+^{207}Tl	35.381	1.6×10^{21}	^{222}Ra$\rightarrow^{18}$O+^{204}Hg	39.938	1.2×10^{28}
^{223}Ra$\rightarrow^{15}$N+^{208}Tl	34.014	1.8×10^{24}	^{223}Ra$\rightarrow^{18}$O+^{205}Hg	40.450	6.7×10^{26}
^{224}Ra$\rightarrow^{20}$O+^{204}Hg	39.860	2.5×10^{29}	^{224}Ra$\rightarrow^{24}$Ne+^{200}Pt	51.549	2.9×10^{34}
^{226}Ra$\rightarrow^{20}$O+^{206}Hg	40.963	3.7×10^{26}	^{226}Ra$\rightarrow^{24}$Ne+^{202}Pt	52.394	1.0×10^{32}
^{225}Ac$\rightarrow^{17}$N+^{208}Pb	35.648	1.6×10^{23}	^{225}Ac$\rightarrow^{18}$O+^{207}Tl	43.602	1.3×10^{21}
^{225}Ac$\rightarrow^{23}$F+^{202}Hg	45.838	5.0×10^{33}	^{225}Ac$\rightarrow^{24}$Ne+^{201}Au	54.170	1.3×10^{30}
^{225}Ac$\rightarrow^{27}$Na+^{198}Pt	57.257	1.2×10^{39}	^{225}Ac$\rightarrow^{28}$Mg+^{197}Ir	65.133	1.7×10^{36}
^{224}Th$\rightarrow^{14}$C+^{210}Po	33.045	1.8×10^{13}	^{224}Th$\rightarrow^{15}$N+^{209}Bi	38.286	3.0×10^{17}
^{224}Th$\rightarrow^{16}$O+^{208}Pb	46.632	6.4×10^{15}	^{224}Th$\rightarrow^{21}$F+^{203}Tl	45.972	7.1×10^{33}
^{224}Th$\rightarrow^{24}$Ne+^{200}Hg	55.634	3.1×10^{29}	^{224}Th$\rightarrow^{28}$Mg+^{196}Pt	67.875	1.3×10^{33}
^{224}Th$\rightarrow^{29}$Al+^{195}Ir	70.134	1.0×10^{42}	^{224}Th$\rightarrow^{32}$Si+^{192}Os	80.200	9.5×10^{35}
^{226}Th$\rightarrow^{14}$C+^{212}Po	30.662	2.0×10^{18}	^{226}Th$\rightarrow^{15}$N+^{211}Bi	35.087	1.6×10^{24}
^{226}Th$\rightarrow^{18}$O+^{208}Pb	45.879	1.5×10^{18}	^{226}Th$\rightarrow^{21}$F+^{205}Tl	47.232	1.1×10^{31}
^{226}Th$\rightarrow^{24}$Ne+^{202}Hg	56.677	8.0×10^{26}	^{226}Th$\rightarrow^{27}$Na+^{199}Au	58.008	2.3×10^{39}
^{226}Th$\rightarrow^{28}$Mg+^{198}Pt	68.335	1.3×10^{32}	^{226}Th$\rightarrow^{32}$Si+^{194}Os	79.954	4.6×10^{35}
^{228}Th$\rightarrow^{14}$C+^{214}Po	28.333	1.1×10^{24}	^{228}Th$\rightarrow^{23}$F+^{205}Tl	47.445	8.3×10^{31}
^{228}Th$\rightarrow^{24}$Ne+^{204}Hg	57.591	2.7×10^{25}	^{228}Th$\rightarrow^{28}$Mg+^{200}Pt	68.600	4.3×10^{31}
^{229}Th$\rightarrow^{14}$C+^{215}Po	27.223	1.1×10^{27}	^{229}Th$\rightarrow^{16}$N+^{213}Bi	29.268	3.3×10^{40}
^{226}Th$\rightarrow^{21}$O+^{208}Pb	43.425	2.2×10^{25}	^{229}Th$\rightarrow^{23}$F+^{206}Tl	48.699	3.3×10^{29}
^{229}Th$\rightarrow^{24}$Ne+^{205}Hg	58.010	7.2×10^{24}	^{229}Th$\rightarrow^{28}$Mg+^{201}Pt	68.561	9.4×10^{30}
^{231}Pa$\rightarrow^{22}$O+^{209}Bi	42.557	2.5×10^{29}	^{231}Pa$\rightarrow^{27}$Na+^{204}Hg	63.837	2.2×10^{29}
^{231}Pa$\rightarrow^{28}$Mg+^{203}Au	71.807	2.6×10^{27}	^{231}Pa$\rightarrow^{31}$Al+^{200}Pt	75.216	4.6×10^{33}
^{232}Pa$\rightarrow^{25}$Ne+^{207}Tl	59.223	2.9×10^{24}	^{232}Pa$\rightarrow^{27}$Na+^{205}Hg	63.951	1.8×10^{29}
^{232}Pa$\rightarrow^{28}$Mg+^{204}Au	71.929	2.1×10^{27}	^{230}U$\rightarrow^{14}$C+^{216}Rn	28.459	1.1×10^{26}
^{230}U$\rightarrow^{20}$O+^{210}Po	43.928	1.5×10^{26}	^{230}U$\rightarrow^{21}$F+^{209}Bi	50.095	5.7×10^{27}
^{230}U$\rightarrow^{24}$Ne+^{206}Pb	61.543	9.3×10^{21}	^{230}U$\rightarrow^{27}$Na+^{203}Tl	63.101	1.9×10^{32}
^{230}U$\rightarrow^{28}$Mg+^{202}Hg	74.201	1.4×10^{25}	^{230}U$\rightarrow^{32}$Si+^{198}Pt	85.851	7.7×10^{29}
^{232}U$\rightarrow^{23}$F+^{209}Bi	49.728	9.4×10^{29}	^{232}U$\rightarrow^{27}$Na+^{205}Tl	64.151	3.5×10^{30}
^{232}U$\rightarrow^{28}$Mg+^{204}Hg	74.537	7.9×10^{24}	^{232}U$\rightarrow^{32}$Si+^{200}Pt	85.537	3.8×10^{29}
^{233}U$\rightarrow^{27}$Na+^{206}Tl	64.900	2.1×10^{29}	^{233}U$\rightarrow^{28}$Mg+^{205}Hg	74.451	1.5×10^{25}
^{234}U$\rightarrow^{27}$Na+^{207}Tl	64.907	3.2×10^{29}	^{235}U$\rightarrow^{29}$Mg+^{206}Hg	72.694	2.9×10^{28}
^{225}Np$\rightarrow^{12}$C+^{213}Fr	35.263	2.4×10^{10}	^{225}Np$\rightarrow^{14}$C+^{211}Fr	32.830	3.1×10^{16}
^{225}Np$\rightarrow^{16}$O+^{209}At	49.367	5.3×10^{14}	^{227}Np$\rightarrow^{14}$C+^{213}Fr	33.217	1.2×10^{16}
^{227}Np$\rightarrow^{16}$O+^{211}At	49.106	1.9×10^{15}	^{227}Np$\rightarrow^{17}$O+^{210}At	45.502	1.3×10^{22}
^{227}Np$\rightarrow^{18}$O+^{209}At	46.387	1.0×10^{21}	^{229}Np$\rightarrow^{18}$O+^{211}At	46.369	1.8×10^{21}

Table 3. The same as Table 2

^{231}Np→^{20}O+^{211}At	43.636	1.7×10^{28}	^{231}Np→^{22}Ne+^{209}Bi	62.103	1.3×10^{21}
^{233}Np→^{22}Ne+^{211}Bi	58.028	9.4×10^{27}	^{233}Np→^{24}Ne+^{209}Bi	62.355	1.1×10^{22}
^{233}Np→^{25}Ne+^{208}Bi	59.075	6.4×10^{27}	^{234}Np→^{24}Ne+^{209}Bi	60.897	1.8×10^{24}
^{234}Np→^{28}Mg+^{206}Tl	77.458	5.2×10^{22}	^{235}Np→^{28}Mg+^{207}Tl	77.326	1.0×10^{23}
^{235}Np→^{29}Mg+^{206}Tl	74.131	1.1×10^{28}	^{236}Np→^{28}Mg+^{208}Tl	75.372	8.0×10^{24}
^{236}Np→^{29}Mg+^{207}Tl	75.238	3.1×10^{26}	^{236}Np→^{30}Mg+^{206}Tl	74.747	3.8×10^{27}
^{237}Np→^{32}Si+^{205}Au	88.120	1.8×10^{28}	^{234}Pu→^{24}Ne+^{210}Po	62.453	2.9×10^{23}
^{234}Pu→^{27}Na+^{207}Bi	66.138	7.2×10^{30}	^{234}Pu→^{28}Mg+^{206}Pb	79.386	5.4×10^{21}
^{234}Pu→^{29}Al+^{205}Tl	82.634	1.4×10^{27}	^{234}Pu→^{32}Si+^{202}Hg	92.037	1.8×10^{24}
^{236}Pu→^{24}Ne+^{212}Po	59.417	3.7×10^{28}	^{236}Pu→^{27}Na+^{209}Bi	66.890	8.2×10^{28}
^{236}Pu→^{29}Al+^{207}Tl	82.395	5.1×10^{27}	^{236}Pu→^{32}Si+^{204}Hg	91.929	4.8×10^{24}
^{237}Pu→^{29}Mg+^{208}Pb	77.679	6.7×10^{23}	^{237}Pu→^{30}Al+^{207}Tl	82.250	1.7×10^{28}
^{237}Pu→^{32}Si+^{205}Hg	91.725	1.0×10^{25}	^{238}Pu→^{31}Al+^{207}Tl	82.404	3.0×10^{28}
^{237}Am→^{28}Mg+^{209}Bi	80.086	7.8×10^{21}	^{237}Am→^{29}Mg+^{208}Bi	76.282	3.3×10^{27}
^{237}Am→^{32}Si+^{205}Tl	94.740	1.0×10^{23}	^{238}Am→^{28}Mg+^{210}Bi	78.473	1.4×10^{24}
^{238}Am→^{29}Mg+^{209}Bi	77.524	6.6×10^{25}	^{238}Am→^{32}Si+^{206}Tl	95.026	5.4×10^{22}
^{238}Am→^{33}Si+^{205}Tl	93.030	3.0×10^{25}	^{239}Am→^{30}Mg+^{209}Bi	76.782	2.1×10^{27}
^{239}Am→^{32}Si+^{207}Tl	94.775	1.3×10^{23}	^{239}Am→^{33}Si+^{207}Tl	92.431	2.5×10^{26}
^{239}Am→^{34}Si+^{205}Tl	93.441	1.9×10^{25}	^{240}Am→^{33}Si+^{207}Tl	93.331	1.9×10^{25}
^{240}Am→^{34}Si+^{206}Tl	93.994	4.6×10^{24}	^{241}Am→^{33}Si+^{208}Tl	90.474	1.4×10^{29}
^{241}Am→^{34}Si+^{207}Tl	94.198	2.6×10^{24}	^{238}Cm→^{28}Mg+^{210}Po	80.659	6.2×10^{22}
^{238}Cm→^{32}Si+^{206}Pb	97.583	2.7×10^{21}	^{239}Cm→^{32}Si+^{207}Pb	97.954	1.4×10^{21}
^{240}Cm→^{30}Mg+^{210}Po	76.808	1.2×10^{29}	^{240}Cm→^{32}Si+^{208}Pb	97.822	1.8×10^{20}
^{240}Cm→^{34}Si+^{206}Pb	95.738	1.9×10^{24}	^{241}Cm→^{32}Si+^{209}Pb	95.673	7.3×10^{22}
^{242}Cm→^{32}Si+^{210}Pb	93.889	1.3×10^{25}	^{242}Cm→^{34}Si+^{208}Pb	96.788	8.2×10^{21}
^{243}Cm→^{34}Si+^{209}Pb	95.032	1.2×10^{24}	^{243}Cm→^{34}Si+^{210}Pb	93.416	1.5×10^{26}
^{242}Cf→^{32}Si+^{210}Po	99.704	3.4×10^{21}	^{242}Cf→^{33}Si+^{209}Po	96.554	3.7×10^{25}
^{242}Cf→^{34}Si+^{208}Po	97.100	1.4×10^{25}	^{242}Cf→^{36}S+^{206}Pb	114.156	8.4×10^{22}
^{244}Cf→^{34}Si+^{210}Po	97.671	2.9×10^{24}	^{244}Cf→^{36}S+^{208}Pb	114.206	5.0×10^{21}
^{246}Cf→^{38}S+^{208}Pb	113.023	1.6×10^{23}	^{249}Cf→^{42}S+^{207}Pb	110.177	3.1×10^{27}
^{249}Cf→^{46}Ar+^{203}Hg	125.077	6.7×10^{26}	^{249}Cf→^{48}Ca+^{201}Pt	138.071	2.4×10^{26}
^{249}Cf→^{50}Ca+^{199}Pt	137.085	5.5×10^{27}	^{251}Cf→^{46}Ar+^{205}Hg	126.505	8.6×10^{24}
^{250}No→^{48}Ca+^{202}Pb	152.135	1.1×10^{19}	^{251}No→^{48}Ca+^{203}Pb	152.184	1.1×10^{19}
^{252}No→^{48}Ca+^{204}Pb	152.614	3.9×10^{18}	^{252}No→^{50}Ca+^{202}Pb	148.805	1.2×10^{23}
^{253}No→^{48}Ca+^{205}Pb	152.767	1.3×10^{17}	^{253}No→^{50}Ca+^{203}Pb	149.148	4.5×10^{22}
^{254}No→^{48}Ca+^{206}Pb	153.147	5.5×10^{16}	^{254}No→^{50}Ca+^{204}Pb	149.836	2.5×10^{20}
^{255}No→^{48}Ca+^{207}Pb	153.895	1.6×10^{16}	^{255}No→^{50}Ca+^{205}Pb	150.578	2.1×10^{19}
^{256}No→^{48}Ca+^{208}Pb	154.210	7.1×10^{15}	^{256}No→^{50}Ca+^{206}Pb	151.611	1.0×10^{18}

Table 4. The same as Table 2

^{257}No$\rightarrow^{48}$Ca+^{209}Pb	152.502	1.1×10^{17}	^{257}No$\rightarrow^{50}$Ca+^{207}Pb	152.704	8.9×10^{16}
^{258}No$\rightarrow^{48}$Ca+^{210}Pb	150.844	9.3×10^{18}	^{258}Rf$\rightarrow^{48}$Ca+^{210}Po	156.949	3.6×10^{16}
^{258}Rf$\rightarrow^{49}$Ca+^{209}Po	154.437	3.5×10^{19}	^{258}Rf$\rightarrow^{50}$Ca+^{208}Po	153.830	1.5×10^{20}
^{258}Rf$\rightarrow^{51}$Ti+^{207}Pb	168.987	1.0×10^{18}	^{258}Rf$\rightarrow^{52}$Ti+^{206}Pb	170.058	2.7×10^{16}
^{258}Rf$\rightarrow^{53}$Ti+^{205}Pb	167.404	4.7×10^{19}	^{258}Rf$\rightarrow^{54}$Ti+^{204}Pb	167.508	2.5×10^{19}

References

[1] Sandulescu A,Poenaru D N and Greiner W 1980 Sov J. Part. Nucl. **11**, 528.
[2] Rose H J, Jones G A 1984 Nature **307** 245.
[3] Aleksandrov D V, Belyatskii A F, Glukhov Yu A et al 1984 JETP Lett.**40** 909.
[4] Poenaru D N, Ivascu M, Sandulescu A and Greiner W 1984 J. Phys. G: Nucl. Part. Phys. **10** L183.
[5] Greiner W, Ivascu M, Poenaru D N and Sandulescu A, Z 1985 Phys. A **320** 347.
[6] Royer G, Gupta R K and Denisov V Y 1988 Nucl.Phys. A **632**, 275.
[7] Royer G and Moustabchir R 2001 Nucl.Phys.A **683**,182.
[8] Kumar S,Balasubramaniam M, Gupta R K et al 2003 J. Phys. G: Nucl. Part. Phys. **29**, 625.
[9] Kumar S, Rani R and Kumar R 2009 J. Phys. G: Nucl. Part. Phys. **36**, 015110.
[10] Balasubramaniam M and Gupta R K 1999 Phys. Rev. C **60**, 064316 .
[11] Xu F R and Pei J C 2006 Phys. Lett. B **642**, 322.
[12] Royer G and Remaud B, 1984 J. Phys. G: Nucl. Part. Phys. 10, 1057.
[13] Royer G, REMAUD B 1985 Nucl.Phys. A **444** 477.
[14] Royer G, 2000 J. Phys. G: Nucl. Part. Phys. 26, 1149.
[15] Royer G and Moustabchir R 2001 Nucl.Phys.A **683**,182.
[16] Royer G and Gherghescu R A 2002 Nucl. Phys. A **699**, 479.
[17] Royer G, Zbiri K and Bonilla C 2004 Nucl. Phys. A **730**, 355.
[18] Zhang Hongfei, Zuo Wei, Li Junqing and Royer G 2006 Phys. Rev. C **74**, 017304.
[19] Royer G and Zhang H F 2008 Phys. Rev. C **77**, 037602.
[20] Zhang H F , Dong J M, Royer G, Zuo W and Li J Q 2009 PRC **80**, 037307.
[21] Royer G and Remaud B 1982 J.Phys.G:Nucl.Phys. **8** L159-L164.
[22] Blocki J, Randrup J, Swiatecki W J, Tsang C F 1977 Ann.of Physics **105** 427.
[23] Royer G, Gupta Raj K, Denisov V Yu 1998 Nuclear Physics A **632** 275-284.
[24] Blendowske R and Walliser H,1988 Phys. Rev. Lett. **61**, 1930.
[25] Bonilla C and Royer G 2006 Acta Physica Hungarica A **25** 11.
[26] Wang Ning, Liu Min and Wu Xizhen 2010 Phys Rev C 81, 044322.
[27] Wang Ning and Liu Min 2010 Phys Rev C 81,067302.
[28] Moller P, Nix J R, Myers W D and Swiatecki W J, "Nuclear Ground Masses and Deformations," Los Alamos present LA-UR-93-3083, Aug. 16 1993, to be published in the Atomic Data and Nuclear Data Tables.
[29] Shi Y J and Swiatecki W J 1987 Nucl. Phys. A **464** 205.
[30] Zamyatnin Y S et al 1990 Sov J. Part. Nuclei **21**, 537.
[31] Bonetti R, Guglielmetti A, in:Gupta R K, Greiner W(Eds.) 1999 Heavy Elements and Related New Phenomena, World Scientific, Singapore, p.643.
[32] Audi.W and Meng.W(private communication).
[33] Kuklin S N, Adamian G G and Ant N V 2005 Phys Rev C **71**, 014301.
[34] Poenaru D N, Greiner W and Hourani E 1995 Phys. Rev. C **51** 594.